Automatic Tuning of Cascaded Controllers for Power Converters Using Eigenvalue Parametric Sensitivities

Salvatore D'Arco, Jon Are Suul, *Member, IEEE*, and Olav Bjarte Fosso, *Senior Member, IEEE*

***Abstract*—Control structures containing cascaded loops are used in several applications for the stand-alone and parallel operation of three-phase power electronic converters. Potential interactions between these cascaded loops and the complex functional dependence between the controller parameters and the system dynamics prevent the effective application of classical tuning methods in the case of converters operating with a low switching frequency. A tuning approach guided by the eigenvalue parametric sensitivities calculated from a linearized model of the converter and its control system is proposed in this paper. The method is implemented in the form of an iterative procedure enforcing the stability of the system and ensuring that the system eigenvalues are moved away from critical locations. Numerical simulations in the time domain are presented to verify the improvement in the dynamic performance of the system when tuned with the presented algorithm compared with a conventional rule-based tuning method.**

***Index Terms*—Control design, dc–ac power converters, eigenvalues and eigenfunctions, power conversion.**

I. Introduction

AC VOLTAGE controllers are required in several power converter applications for stand-alone and parallel operation, such as uninterruptible power supplies (UPSs) and microgrids [1]–[5]. Such ac voltage control loops can be implemented to directly control the output voltage, as discussed in [3] and [4], but control schemes with inner loop current controllers are often preferred since they allow for explicit limitations and protections against overcurrents. In most applications, the references for these ac voltage controllers are provided by outer loops for ensuring active and reactive power control as well as automatic load sharing among parallel units. Such control schemes may result in a structure with three cascaded loops and a relatively high number of tunable parameters that influence the dynamic response of the system [1], [2].

The controllers in cascaded structures are traditionally independently tuned by frequency-domain analysis, with the inner loops represented by first-order approximations [6]–[8]. Sufficient frequency separation between the bandwidths of the loops, usually in the range of one decade, is then imposed to avoid unintended interactions. Thus, the dynamic response of the outer loops is effectively limited by the bandwidth of the inner current controllers, which is constrained by the switching frequency. This can be affordable for low-power converters with high switching frequencies but can result in a slow response and narrow stability regions for lower switching frequencies. Consequently, the tuning of controller parameters in multiloop control structures for low-switching-frequency converters is challenging and normally includes trial-and-error approaches requiring significant design experience to ensure acceptable dynamic performance over the entire operating range.

A systematic approach for the tuning of the multiloop controllers of power converters should be able to account for all the dynamic states of the system and their possible interactions. This can be achieved by establishing a linearized small-signal state-space model of the system. With this approach, the influence of the controller parameters on the system stability can be assessed by calculating the system eigenvalues and applying tools such as participation factors and eigenvalue parametric sensitivities [9]. Although such tools for small-signal stability analysis are commonly applied for large-scale power systems, they are rarely utilized for multiloop power converter control systems beyond the basic eigenvalue calculation and root loci trajectories applied in [10]–[13].

Examples of participation factor and parameter sensitivity analysis applied to multiloop control structures for ac power converters have been presented in [14]–[16]. Still, the mathematical tools are not actively utilized in these previous studies but only serve as a support for the analysis and manual tuning of controllers. This paper will instead demonstrate how the parametric sensitivities of the eigenvalues of a linearized small-signal system model can be systematically used to identify controller settings that will improve the dynamic response of a given system. Furthermore, an iterative tuning approach for automatically enforcing stability and improving the dynamic response of a multiloop control system within the physical constraints of the system eigenvalue locations is presented, as first proposed in [17].

Manuscript received October 11, 2013; revised April 15, 2014; accepted August 1, 2014. Date of publication September 4, 2014; date of current version March 17, 2015. Paper 2013-IPCC-797.R1, presented at the 2013 IEEE Energy Conversion Congress and Exposition, Denver, CO, USA, September 16–20, and approved for publication in the IEEE TRANSACTIONS ON INDUSTRY APPLICATIONS by the Industrial Power Converter Committee of the IEEE Industry Applications Society. The work of SINTEF Energy Research in this paper was supported by the project "Releasing the Potential of Virtual Synchronous Machines–ReViSM" through the Blue Sky instrument of SINTEF Energy Research as a Strategic Institute Programme (SIP) financed by the national Basic Funding Scheme of Norway.

S. D'Arco is with SINTEF Energy Research, 7465 Trondheim, Norway (e-mail: salvatore.darco@sintef.no).

J. A. Suul is with SINTEF Energy Research, 7565 Trondheim, Norway, and also with the Department of Electric Power Engineering, Faculty of Information Technology, Mathematics and Electrical Engineering, Norwegian University of Science and Technology, 7495 Trondheim, Norway (e-mail: jon.are.suul@elkraft.ntnu.no).

O. B. Fosso is with the Department of Electric Power Engineering, Faculty of Information Technology, Mathematics and Electrical Engineering, Norwegian University of Science and Technology, 7495 Trondheim, Norway (e-mail: olav.fosso@ntnu.no).

Color versions of one or more of the figures in this paper are available online at http://ieeexplore.ieee.org.

Digital Object Identifier 10.1109/TIA.2014.2354732

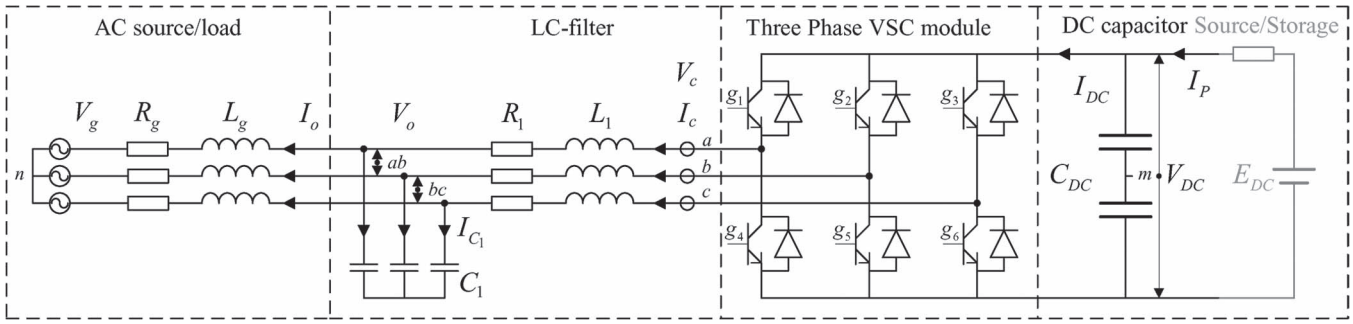

Fig. 1. Schematic of the analyzed converter configuration.

In the following, a virtual synchronous machine (VSM) is taken as an example of a multiloop control system that can be challenging to tune by conventional methods. A traditional approach for selecting the controller parameters by using tuning rules based on single-input–single-output approximations will first be presented as a reference case. A linearized state-space model of the system is developed, and the challenges related to the tuning of this control system configuration with a low switching frequency are demonstrated. Then, the eigenvalue parametric sensitivities are formally defined, and the proposed iterative algorithm is developed. The performance resulting from the tuning with the proposed algorithm is compared with the conventional tuning approach by time-domain simulations, including discretization effects and the switching operation of the converter.

II. Overview of VSM With Cascaded Control Loops

The VSM has recently emerged as a concept for controlling voltage source converters (VSCs) in power system applications to emulate the behavior of traditional synchronous machines (SMs) [18]–[22]. Such VSM-based controllers can allow for grid-connected as well as stand-alone operation and can ensure load sharing in a similar way as droop-based control schemes for UPS systems and microgrids [22].

Although several possible implementations of the VSM concept have been proposed during the last years, control schemes based on cascaded voltage and current controllers present significant advantages regarding the implementation of overcurrent protections [22]. Moreover, it has been recently demonstrated that VSM implementations based on emulating the swing equation of a traditional SM are equivalent to the power-frequency droop controllers commonly used in microgrids [23]. Thus, a VSM can be a relevant example of a control system with outer loop active and reactive power controllers providing references for cascaded voltage and current controllers.

A. Electrical Configuration and System Model

The investigated VSM scheme consists of a three-phase VSC connected to a grid or a load through an LC filter, as shown in Fig. 1. An energy source and/or a storage unit with a buffer capacity at least equivalent to the inertia effect represented by the rotating mass of the emulated SM is assumed to be connected to the dc-terminals of the converter. Symbols and current reference directions are defined in this figure, with upper case symbols denoting the physical variables and parameters.

In the following, switching dynamics are assumed to be negligible for the scope of this analysis, and the converter is represented by a continuous-time average model. Thus, the equations of the converter-side filter inductors in the synchronous reference frame (SRF) can be expressed in the continuous-time Laplace domain, as given by (1), whereas the equations of the filter capacitors are given by (2) [7], [14], as shown in the following:

$$\begin{aligned}\frac{l_1}{\omega_b}\cdot s\cdot i_{c,d} &= v_{c,d} - r_1\cdot i_{c,d} + \omega_g\cdot l_1\cdot i_{c,q} - v_{o,d}\\ \frac{l_1}{\omega_b}\cdot s\cdot i_{c,q} &= v_{c,q} - r_1\cdot i_{c,q} - \omega_g\cdot l_1\cdot i_{c,d} - v_{o,q}\end{aligned} \quad (1)$$

$$\begin{aligned}\frac{c_1}{\omega_b}\cdot s\cdot v_{o,d} &= i_{c,d} + \omega_g\cdot c_1\cdot v_{o,q} - i_{o,d}\\ \frac{c_1}{\omega_b}\cdot s\cdot v_{o,q} &= i_{c,q} - \omega_g\cdot c_1\cdot v_{o,d} - i_{o,q}.\end{aligned} \quad (2)$$

The grid side or load is represented by a Thévenin equivalent RL circuit, which can be represented by a model on the same form as (1). In these equations, all signals and parameters are represented by lower case symbols to denote per unit (p.u.) values, where the base values defining the p.u. system are derived from the kilovoltampere rating of the converter and the peak value of the rated phase voltage. The term ω_b is the base value for the angular frequency in rad/s, corresponding to the rated frequency of the system.

B. VSM-Based Control System

The VSM-based control structure for the converter is shown in Fig. 2. The control system consists of a modulation stage, a traditional SRF current controller as an inner loop, and an SRF voltage controller as an intermediate control loop [14]. The outer control loops consist of a conventional reactive power droop controller and the VSM inertia emulation. Thus, the general structure of the control system is identical to the equivalent droop-based controllers from the work in [1], [2], and [10]–[14] and will not be further described in detail.

In the control structure in Fig. 2, the reference for the q-axis voltage is equal to zero since the SRF is oriented to the voltage at the filter inductors, whereas the d-axis voltage amplitude reference is provided by a conventional droop-based reactive power controller, as shown in the upper left in this figure

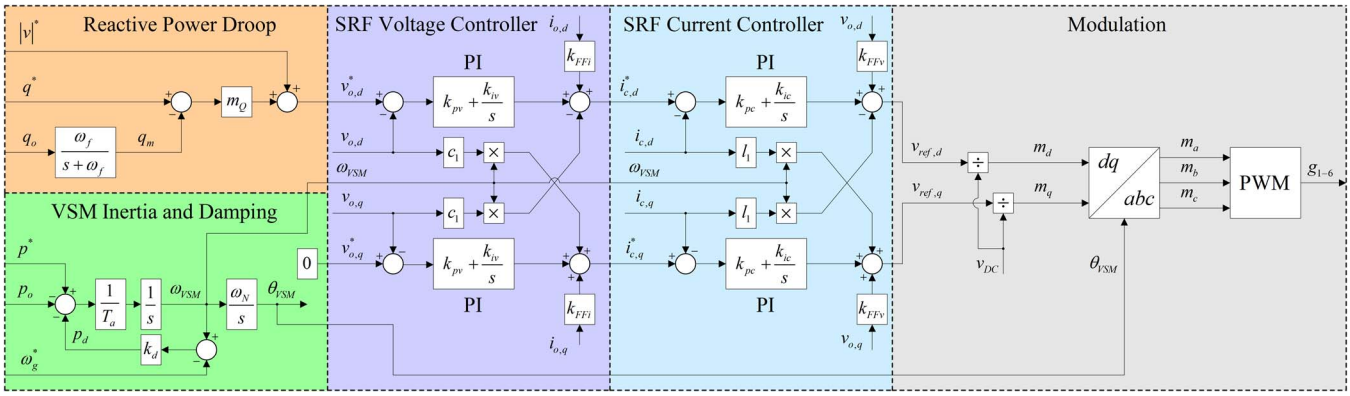

Fig. 2. VSM-based control system with cascaded voltage and current control loops.

[1], [14]. For this controller, $|v|^*$ is the external voltage reference, q^* is the reactive power reference, and q_o is the reactive power flowing into the grid, as defined by

$$q_o = v_{o,q} \cdot i_{o,d} - v_{o,d} \cdot i_{o,q}. \tag{3}$$

The phase angle used for transforming the SRF variables to the stationary reference frame is obtained by integrating the frequency resulting from the inertia and damping emulation according to the swing equation shown in the lower left in Fig. 2 and expressed by

$$T_a \cdot s \cdot \omega_{\mathrm{VSM}} = p^* - \underbrace{k_d(\omega_{\mathrm{VSM}} - \omega_g)}_{p_d} - p_o. \tag{4}$$

In this equation, T_a is the mechanical time constant of the emulated inertia, whereas ω_{VSM} is the p.u. speed of the VSM. The external power reference is given by p^*, whereas damping power p_d is given by damping constant k_d and the difference between the p.u. VSM speed and the p.u. grid angular frequency ω_g. The electrical power flowing into the grid is given by p_o according to

$$p_o = v_{o,d} \cdot i_{o,d} + v_{o,q} \cdot i_{o,q}. \tag{5}$$

If the converter is operated in a grid-connected mode, the VSM control synchronizes to the grid voltage phase angle through the power balance of the swing equation. Thus, the normal operation of the VSM does not depend on any grid synchronization method (e.g., a phase-locked loop) as usually required for grid-connected converters. The VSM is also inherently capable of stand-alone operation similar to a traditional SM. Thus, the control loops are implemented in an SRF defined by the VSM swing equation, which is also used for the modeling of the entire system.

III. Example of Conventional Tuning for Cascaded Voltage and Current Control Loops

In the following, an example of a simple analytical tuning procedure for the VSM voltage and current controllers is outlined according to conventional assumptions and rule-based methods adopted for the design of proportional–integral (PI) controllers in the SRF.

A. Conventional Current Controller Tuning

For tuning the parameters of the inner loop current controllers in Fig. 2, the delay effect of the converter pulsewidth modulated (PWM) operation must be considered. By approximating the effect of the PWM with a first-order transfer function and assuming feedforward of the measured voltages and ideal decoupling of the d- and q-axes, the open-loop transfer function for the current controllers can be defined by (6) [7], [24]. The time constants T_1 for the filter inductor and T_v for the delay approximation are then defined by (7), as shown in the following:

$$h_{cc,\,dq}(s) \approx \underbrace{\left(k_{pc} + \frac{k_{ic}}{s}\right)}_{\text{PI controller}} \cdot \underbrace{\frac{1}{1+T_v \cdot s}}_{\text{PWM approximation}} \cdot \underbrace{\frac{1}{r(1+T_1 \cdot s)}}_{\text{Filter inductor}} \tag{6}$$

$$T_1 = \frac{L_1}{R_1} = \frac{l_1}{r_1 \cdot \omega_b} \qquad T_v \approx \frac{1}{2 \cdot f_{sw}}. \tag{7}$$

Based on the open-loop transfer function in (6), the PI current controller gains can be selected according to the modulus optimum (MO) criterion commonly applied for current controllers in drives and grid-connected converters [6], [7]. This tuning technique corresponds to pole cancelation in the open-loop transfer function and a gain selected to achieve critical damping of the resulting closed-loop transfer function. The resulting controller parameters k_{pc} and k_{ic} are given by

$$k_{pc} = \frac{l_1}{2 \cdot \omega_b \cdot T_v} \qquad k_{ic} = \frac{r_1}{2 \cdot T_v}. \tag{8}$$

This tuning approach can be also extended to account for the sampling effects and the delays resulting from a discrete-time implementation of the control system [8]. In any case, it is clearly seen from the expressions in (8) that the PI controller parameters and, thus, the current controller bandwidth is directly limited by the switching frequency.

B. Conventional Voltage Controller Tuning

From the cascaded structure shown in Fig. 2, it is clear that the tuning of the SRF voltage controllers is constrained by the bandwidth of the inner loop current controllers. For simplifying the analysis, the closed-loop current controllers can be approximated by a first-order transfer function [7]. Assuming an ideal decoupling of the d- and q-axes, the open-loop transfer function of the voltage controllers can be expressed by (9). The time constant $T_{eq,\,cc}$ representing the closed-loop current controller and the integral time T_{c1} of the filter capacitor are defined by (10), as shown in the following:

$$h_{vc,\,dq}(s) \approx \underbrace{\left(k_{pv} + \frac{k_{iv}}{s}\right)}_{\text{PI controller}} \cdot \underbrace{\frac{1}{1 + T_{eq,\,cc} \cdot s}}_{\text{Closed-loop current controller}} \cdot \underbrace{\frac{1}{T_{c_1} \cdot s}}_{\text{Filter capacitor}} \tag{9}$$

$$T_{eq,\,cc} \approx 2 \cdot T_v \qquad T_{c_1} = \frac{c_1}{\omega_b}. \tag{10}$$

The voltage controller parameters can be tuned according to the symmetrical optimum (SO) criterion to ensure maximum phase margin at the crossover frequency of the open-loop transfer function. PI controller gains k_{pv} and k_{iv} are then expressed in terms of a design parameter a that relates the tuning of the PI controller to the damping factor ζ of the closed-loop transfer function as given by [6], [7]

$$k_{pv} = \frac{T_{c_1}}{a \cdot T_{eq,\,cc}}, \qquad k_{iv} = \frac{T_{c_1}}{a^3 \cdot T_{eq,\,cc}^2}, \quad a = 2\zeta + 1. \tag{11}$$

This conventional tuning approach requires sufficient difference in the bandwidth between the outer voltage controller and the inner current controller. Traditionally, this is ensured by increasing the value of a until the bandwidth of the voltage controller is at least one decade below the current controller bandwidth. The SO tuning criterion can be also extended to account for the sampling effects and the delays resulting from a discrete-time implementation [8].

IV. Small-Signal Stability and Eigenvalue Parametric Sensitivity of the VSM Configuration

Considering the VSM scheme in Fig. 2, neither the intended operation of the outer loops for reactive power control and inertia emulation nor the overall system stability will be ensured if the bandwidth of the voltage controller loop is too low. Thus, if the current controller bandwidth is limited due to a relatively low converter switching frequency, significant interactions between the different control loops might occur. This makes it necessary to study the stability and dynamics of the overall system.

A. State-Space System Model

A mathematical model of the VSM can be established by combining the model of the circuit in Fig. 1 with the control system diagram in Fig. 2. This model can be linearized and expressed in standard matrix notation as $\Delta\dot{\boldsymbol{x}} = \boldsymbol{A} \cdot \boldsymbol{\Delta x} + \boldsymbol{B} \cdot \boldsymbol{\Delta u}$, where the $\boldsymbol{A}$ matrix and state variables $\boldsymbol{x}$ are defined by (12), shown at bottom of the next page, whereas the $\boldsymbol{B}$ matrix and input variables $\boldsymbol{u}$ are given by

$$\mathbf{B} = \begin{bmatrix} 0 & 0 & 0 & 0 & 0 & 0 \\ 0 & 0 & 0 & 0 & 0 & -\omega_b v_{o,\,d,\,0} \\ 0 & m_q & 0 & 1 & 0 & 0 \\ 0 & 0 & 0 & 0 & 0 & 0 \\ 0 & \frac{k_{pc} k_{pv} m_q}{\frac{l_1}{\omega_b}} & 0 & \frac{k_{pc} k_{pv}}{\frac{l_1}{\omega_b}} & 0 & 0 \\ 0 & 0 & 0 & 0 & 0 & \frac{k_{pc} c_1 v_{o,\,d,\,0}}{\frac{l_1}{\omega_b}} \\ 0 & k_{pv} m_q & 0 & k_{pv} & 0 & 0 \\ 0 & 0 & 0 & 0 & 0 & c_1 v_{o,\,d,\,0} \\ 0 & 0 & \frac{-\cos\delta\theta_{\mathrm{VSM},0}}{\frac{l_g}{\omega_b}} & 0 & 0 & \omega_b i_{o,\,q,0} \\ 0 & 0 & \frac{\sin\delta\theta_{\mathrm{VSM},0}}{\frac{l_g}{\omega_b}} & 0 & 0 & -\omega_b i_{o,\,d,\,0} \\ 0 & 0 & 0 & 0 & 0 & 0 \\ \frac{1}{T_a} & 0 & 0 & 0 & \frac{k_d}{T_a} & -\frac{k_d}{T_a} \\ 0 & 0 & 0 & 0 & 0 & 0 \end{bmatrix}$$

$$\Delta\mathbf{u} = \begin{bmatrix} \Delta p^* & \Delta q^* & \Delta\hat{v}_g & \Delta|v|^* & \Delta\omega_g^* & \Delta\omega_g \end{bmatrix}^T. \tag{13}$$

In this state-space model, the state variables represent small-signal deviations around an operating point, and the values of variables referring to this operating point are denoted with 0 as subscript [9]. Auxiliary variables ξ and σ are introduced to represent the states of the integrators in the SFR current and voltage controllers. The state variable $\delta\theta_{\mathrm{VSM}}$ is introduced to represent the small-signal variations in the phase shift between the VSM phase angle orientation and the phase angle of the grid voltage when the system is modeled in the VSM-oriented SRF. Thus, this state variable is defined by

$$s \cdot \delta\theta_{\mathrm{VSM}} = \delta\omega_{\mathrm{VSM}} \cdot \omega_b = (\omega_{\mathrm{VSM}} - \omega_g)\omega_b \tag{14}$$

where $\delta\omega_{\mathrm{VSM}}$ is the small-signal deviation of the VSM speed from the actual grid angular frequency. The initial condition of this state variable is directly given by the initial phase angle between the VSM orientation and the grid source voltage according to $\delta\theta_{\mathrm{VSM},\,0} = \theta_{\mathrm{VSM},\,0} - \theta_{g,\,0}$.

B. System Stability by Eigenvalue Analysis

The stability behavior of the VSM can be assessed by performing an analysis of the eigenvalues of the $\mathbf{A}$ matrix in (12) for various operating points and combinations of control parameters. In the following, an example of analysis based on the parameters in Table I and the tuning approach from Section III is presented. For this analysis, the voltage feedforward is assumed to be enabled by setting $k_{\mathrm{FF}v} = 1$, whereas the current feedforward is disabled by setting $k_{\mathrm{FF}i} = 0$. The reactive power droop gain m_q is set to a very low value, effectively disabling the loop in this case.

The trajectories of the system eigenvalues in the complex plane when the design parameter a for tuning the voltage loop is swept from 0.5 to 50 are shown in Fig. 3. This figure shows

TABLE I
SYSTEM PARAMETERS

Parameter	Value	Parameter	Value
Rated voltage $V_{S,LL,RMS}$	690 V	Filter resistance r_f	0.003 pu
Rated power S_b	1 MVA	Filter inductance l_f	0.10 pu
Rated grid frequency f_n	50 Hz	Filter capacitance c_f	0.20 pu
Inertia constant T_a	2 s	Source resistance r_g	0.003 pu
Damping coefficient k_d	10^4 pu	Source inductance l_g	0.10 pu
Power reference, p^*	0.4 pu	Reactive power reference q^*	0.0 pu
Voltage reference $\|v\|^*$	1.0 pu	Reactive power droop gain m_q	$4{\cdot}10^{-5}$ pu
Grid voltage $\|v_g\|$	1.0 pu	Grid frequency, ω_g	1.0 pu

three cases, each designed according to the conventional tuning described in the previous section but with different values of the switching frequency. The poles are marked with black crosses when the system is unstable, whereas arrows indicate the direction of the parameter sweep. This figure shows that the system has a very narrow range of stable operation when the switching frequency is 2 kHz, which is a realistic value for a 690-V converter in the megawatt power range. If the switching frequency is increased to 5 kHz, the system has a significantly wider range of stable operation but can still become unstable if the voltage control loops have either too low damping or is too slow. When increasing the switching frequency to 10 kHz, the system shows a quite wide range of stable operation and becomes unstable only if the voltage control loops are made too slow. This confirms that the conventional tuning approach is most suitable for low-power converters with a high switching frequency (e.g., for small-scale microgrid applications in the kilowatt range).

This eigenvalue analysis reveals how the stability is strongly affected by the achievable bandwidth of the inner loop current controllers and, therefore, by the switching frequency of the converter. Moreover, the described conventional tuning approach can result in poor dynamics and low stability margins when this VSM scheme is operated at a relatively low switching frequency since the control loops cannot be sufficiently decoupled. Although the individual controllers are designed to be stable, their interactions negatively affect the system stability, resulting in a narrow range of stable operation. Therefore, such tuning techniques should be only used as a starting point, whereas the analysis of the full-order model should be adopted to obtain better dynamic performance.

C. Eigenvalue Parametric Sensitivity

The parameter sensitivities of the poles are defined as the derivative of the system eigenvalues with respect to the system parameters. Thus, these parameter sensitivities can identify the parameters with the strongest influence on the critical eigenvalues of the system and can reveal how modifying these parameters will influence the eigenvalue locations [9]. Assuming a dynamic system of order N and a set of K tunable parameters, the sensitivities define a sensitivity matrix of N by K complex elements. The sensitivity $\alpha_{n,k}$ of the eigenvalue λ_n with respect to the parameter ρ_k can be expressed by

$$\alpha_{n,k} = \frac{\partial \lambda_n}{\partial \rho_k} = \frac{\boldsymbol{\Phi}_n^T \frac{\partial \mathbf{A}}{\partial \rho_k} \boldsymbol{\Psi}_n}{\boldsymbol{\Phi}_n^T \boldsymbol{\Psi}_n} \tag{15}$$

where $\boldsymbol{\Psi}_n^T$ and $\boldsymbol{\Psi}_n$ are the left and right eigenvectors, respectively, associated to eigenvalue λ_n [9], [25].

The real and imaginary parts of the sensitivities are associated to the derivatives of the pole location along the real and imaginary axes, respectively. Since the real parts of the pole locations characterize the stability of the system, only the real part of the sensitivity matrix will be investigated in the following.

Two examples of parameter sensitivity analysis are shown in Fig. 4, with reference to a configuration based on the parameters in Table I and the controllers tuned according to (8) and (9), with a equal to 4. This configuration is close to the stability limit and has three pairs of complex conjugate poles close to the imaginary axis. The eigenvalue parametric sensitivities with respect to 15 of the system parameters are plotted in Fig. 4(a)

$$\mathbf{A} = \begin{bmatrix}
0 & \omega_b\omega_{g,0} & 0 & 0 & \frac{\omega_b}{c_1} & 0 & 0 & 0 & -\frac{\omega_b}{c_1} & 0 & 0 & 0 & 0 \\
-\omega_b\omega_{g,0} & 0 & 0 & 0 & 0 & \frac{\omega_b}{c_1} & 0 & 0 & 0 & -\frac{\omega_b}{c_1} & 0 & -\omega_b v_{o,d,0} & 0 \\
-1 & 0 & 0 & 0 & 0 & 0 & 0 & 0 & 0 & 0 & -m_q & 0 & 0 \\
0 & -1 & 0 & 0 & 0 & 0 & 0 & 0 & 0 & 0 & 0 & 0 & 0 \\
\frac{-1-k_{pc}k_{pv}+k_{FFv}}{\frac{l_1}{\omega_b}} & -\frac{k_{pc}c_1\omega_{g,0}}{\frac{l_1}{\omega_b}} & \frac{k_{pc}k_{iv}}{\frac{l_1}{\omega_b}} & 0 & -\frac{k_{pc}+r_1}{\frac{l_1}{\omega_b}} & 0 & \frac{k_{ic}}{\frac{l_1}{\omega_b}} & 0 & \frac{k_{FFi}k_{pc}}{\frac{l_1}{\omega_b}} & 0 & -\frac{k_{pc}k_{pv}m_q}{\frac{l_1}{\omega_b}} & 0 & 0 \\
\frac{k_{pc}c_1\omega_{g,0}}{\frac{l_1}{\omega_b}} & \frac{-1-k_{pc}k_{pv}+k_{FFv}}{\frac{l_1}{\omega_b}} & 0 & \frac{k_{pc}k_{iv}}{\frac{l_1}{\omega_b}} & 0 & -\frac{k_{pc}+r_1}{\frac{l_1}{\omega_b}} & 0 & \frac{k_{ic}}{\frac{l_1}{\omega_b}} & 0 & \frac{k_{FFi}k_{pc}}{\frac{l_1}{\omega_b}} & 0 & \frac{k_{pc}c_1v_{o,d,0}}{\frac{l_1}{\omega_b}} & 0 \\
-k_{pv} & -c_1\omega_{g,0} & k_{iv} & 0 & -1 & 0 & 0 & 0 & k_{FFi} & 0 & -k_{pv}m_q & 0 & 0 \\
c_1\omega_{g,0} & -k_{pv} & 0 & k_{iv} & 0 & -1 & 0 & 0 & 0 & k_{FFi} & 0 & c_1v_{o,d,0} & 0 \\
\frac{1}{\frac{l_g}{\omega_b}} & 0 & 0 & 0 & 0 & 0 & 0 & 0 & -\frac{r_g}{\frac{l_g}{\omega_b}} & \omega_b\omega_{g,0} & 0 & \omega_b i_{o,q,0} & \frac{\hat{v}_{g,0}\sin\delta\theta_{\mathrm{VSM},0}}{\frac{l_g}{\omega_b}} \\
0 & \frac{1}{\frac{l_g}{\omega_b}} & 0 & 0 & 0 & 0 & 0 & 0 & -\omega_b\omega_{g,0} & -\frac{r_g}{\frac{l_g}{\omega_b}} & 0 & -\omega_b i_{o,d,0} & \frac{\hat{v}_g\cos\delta\theta_{\mathrm{VSM},0}}{\frac{l_g}{\omega_b}} \\
-\omega_f i_{o,q,0} & \omega_f i_{o,d,0} & 0 & 0 & 0 & 0 & 0 & 0 & 0 & -\omega_f v_{o,d,0} & -\omega_f & 0 & 0 \\
-\frac{i_{o,d,0}}{T_a} & -\frac{i_{o,q,0}}{T_a} & 0 & 0 & 0 & 0 & 0 & 0 & -\frac{v_{o,d,0}}{T_a} & 0 & 0 & -\frac{k_d}{T_a} & 0 \\
0 & 0 & 0 & 0 & 0 & 0 & 0 & 0 & 0 & 0 & 0 & \omega_b & 0
\end{bmatrix}$$

$$\Delta\mathbf{x} = \begin{bmatrix} \Delta v_{o,d} & \Delta v_{o,q} & \Delta\xi_d & \Delta\xi_q & \Delta i_{c,d} & \Delta i_{c,q} & \Delta\sigma_d & \Delta\sigma_q & \Delta i_{o,d} & \Delta i_{o,q} & \Delta q_m & \Delta\delta\omega_{\mathrm{VSM}} & \Delta\delta\theta_{\mathrm{VSM}} \end{bmatrix}^T \tag{12}$$

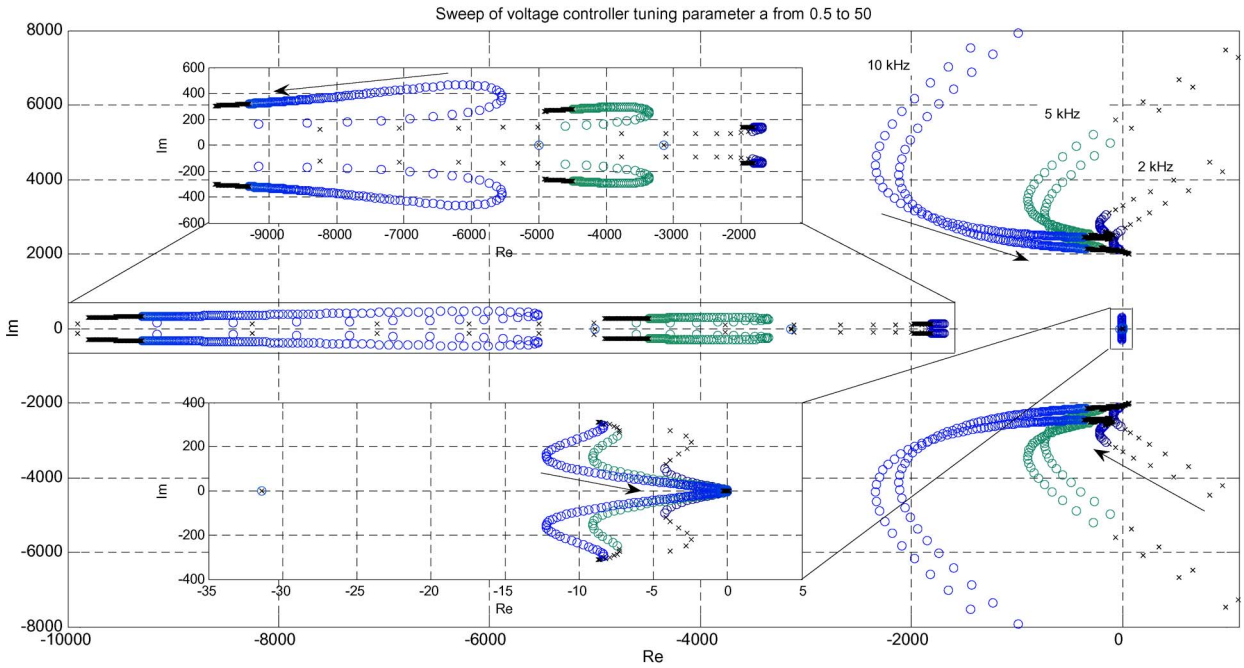

Fig. 3. Effect of design parameter a in the range from 0.5 to 50 on the system stability for various switching frequencies.

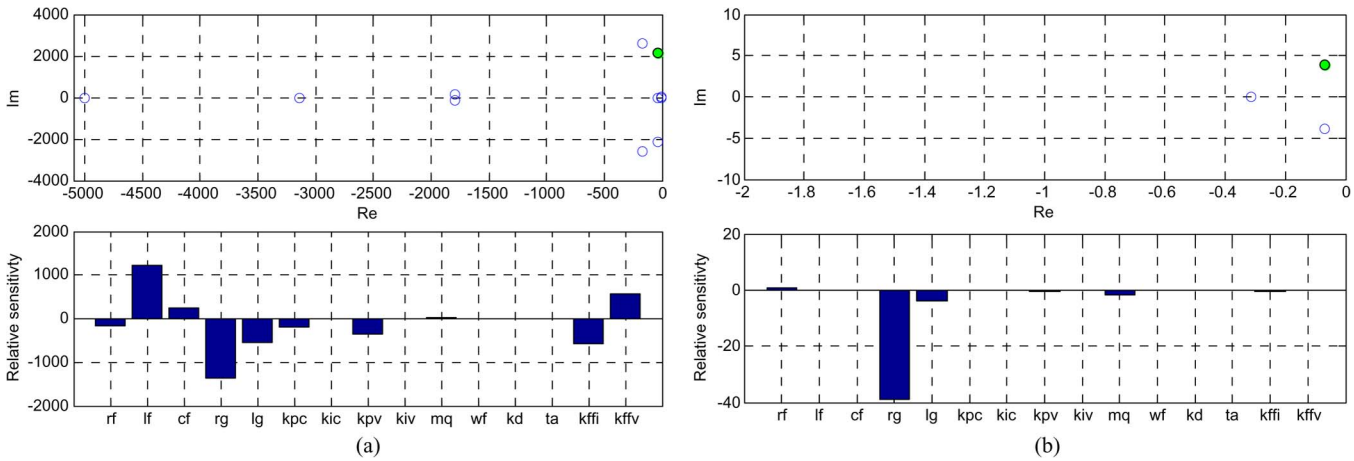

Fig. 4. Parameter sensitivity analysis for, (a), the eigenvalue with a high oscillation frequency related to the LC filter, and (b), for the slowest complex eigenvalue in the system, with conventional tuning and $a = 4$ used for the tuning of the voltage control loop.

for the pole with a high oscillation frequency closest to the imaginary axis. As shown in this figure, the location of this eigenvalue can be influenced by controller parameters k_{pc} and k_{pv}. The LC filter parameters and the grid-side RL circuit, as well as the voltage and current feedforward gains $k_{\mathrm{FF}v}$ and $k_{\mathrm{FF}i}$, are also strongly influencing this mode. There is, however, a pole pair with a low oscillation frequency that is even closer to the imaginary axis than the LC-related poles, and the parametric sensitivity of this pole pair is shown in Fig. 4(b). In this case, the parameters of the grid impedance have a dominant influence, but the eigenvalue is also influenced by k_{pv} and m_q.

V. Algorithm for Stability Enforcement and Parameter Tuning of VSM

The information contained in the parameter sensitivity matrix can be systematically used to establish procedures for designing and tuning the system. An example of such an automated procedure applied to the VSM tuning is described in this section. The tuning is based on an iterative process where the controller parameters are modified at each step to move the poles toward a more convenient location. The iterative process is illustrated by the flowchart in Fig. 5. In the first step, the system parameters and an initial set of controller settings, for instance from a conventional tuning procedure, are taken as a starting point. Then, the steady-state operating point is calculated by solving a system of algebraic equations. It should be noted that the solution may correspond to an unstable operating point, but the instability of the system does not affect the tuning process. As a following step, the dynamic matrix $\mathbf{A}$ for the linearized system around this operating point and its eigenvalues are calculated. In this implementation example, the eigenvalue with the highest real part is considered the critical pole λ_c and is selected as target for the subsequent optimization step. The algorithm proceeds with calculating the parameter sensitivity $\alpha_{c,k}$ of this critical pole with respect to all the system parameters.

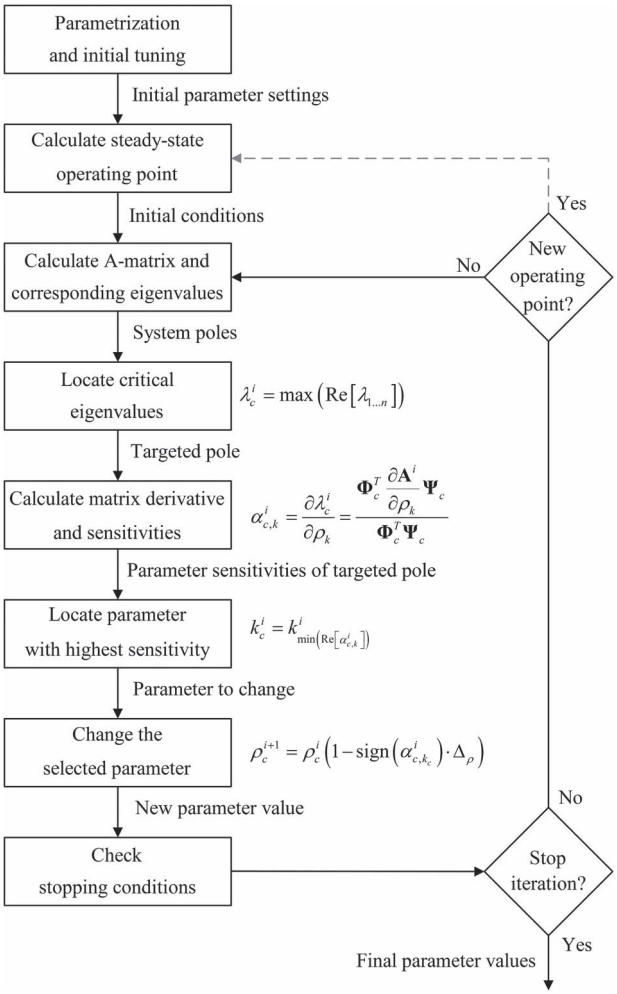

Fig. 5. Flowchart of the proposed algorithm for forcing the system poles into more stable conditions.

Sensitivities for the parameters that are assumed fixed or not tunable are calculated, but the corresponding parameters are left unchanged by the algorithm. Parameter ρ_c for which the critical pole has the highest sensitivity is then changed by an incremental ratio Δ_ρ for each iteration, i.e., i, as given by

$$\rho_c^{i+1} = \rho_c^i \left(1 - \mathrm{sign}\left(\alpha_{c,\,k_c}^i\right) \cdot \Delta_\rho\right). \tag{16}$$

The sign of the sensitivity determines if the parameter would be increased or decreased in order to force a shift of the target pole toward the left. The initial set of parameters is then updated, resulting in a dynamic system with a modified set of poles. In general, the process can be reiterated or terminated according to a predefined termination criterion. This criterion can be a certain maximum settling time, corresponding to a certain real value of the critical eigenvalue. Alternatively, a requirement on the damping ratio of the critical eigenvalue can be set as the criteria for a desired tuning of the system. Since physical constraints to the pole locations are also present in the system, the iterations should be also stopped if the critical pole cannot be moved further toward the left.

For the sake of simplicity, the algorithm is executed for a fixed number of iterations in this implementation example. The modified set of parameters ensures that the pole assumed as the most critical pole will be moved to a location with a lower real part. Although more advanced criteria for changing the system parameters can be considered, this simple condition of the algorithm will ensure that the system dynamics are improved, since poles causing instability will be gradually moved into the stable region while the behavior of slow poles will be improved by forcing the eigenvalues toward the left. However, it should be noted that a modification of certain parameters can move other poles in the opposite direction, resulting in several poles with an almost identical real part. If this condition occurs, the algorithm might exhibit an oscillatory behavior in the sense tshat it alternates between different critical poles that are identified for each iteration cycle. If possible, the different critical poles will be alternately moved toward the left every time they are addressed in an iteration until a condition is reached when the sensitivities of two or more poles to the same parameter are equal in magnitude and opposite in direction.

It can be also noted that the definition of the tunable parameters can be limited to controller gains or can be expanded to include physical parameters (e.g., filter inductance, filter capacitance, etc.). In this perspective, the presented algorithm can be used in an earlier stage of the design of a system, as well as in the more strict sense of control system tuning that has motivated this paper.

VI. Tuning Algorithm Applied to VSM and Verification by Time-Domain Simulations

The VSM scheme in Figs. 1 and 2 has been tuned by the iterative algorithm described in the previous section, and the performance has been compared with the more conventional tuning methodology described in Section III. A subset of seven parameters has been set as tunable $(k_{pc}, k_{pv}, k_{ic}, k_{iv}, \omega_{f,\,pu}, T_a, k_d)$, and they are allowed to be modified by the algorithm. In this case, the algorithm is allowed to modify each parameter by a ratio Δ_ρ of 0.5% for each iteration.

A. Resulting Impact on System Eigenvalue Locations

The starting point for applying the iterative tuning algorithm in the following is the same as for Fig. 4. The impact of the iterative process on the location of the poles is illustrated in Fig. 6(a) and (b), where the shift of the poles is highlighted with a color gradient (from blue to red). These trajectories highlight how the poles closest to the imaginary axis are gradually shifted toward the left, leading to faster dynamics and a more stable behavior. In particular, the zoom in Fig. 6(b) shows how the critical eigenvalues are moved toward the left. The iterations start by moving the critical pole pair in Fig. 4(b), but when these poles are moved toward the left, a slow real pole becomes the limit for the performance of the system. Thus, the algorithm attempts to simultaneously move all the three slowest eigenvalues toward the left by alternatingly changing several of the tunable parameters of the system.

The curves presented in Fig. 6(c) indicate how two of the tunable parameters are modified when executing the algorithm. In particular, the integral gain k_{iv} of the voltage controller is left unchanged for more than 200 iterations, whereas the proportional gain k_{pv} is increased. Subsequently, the algorithm

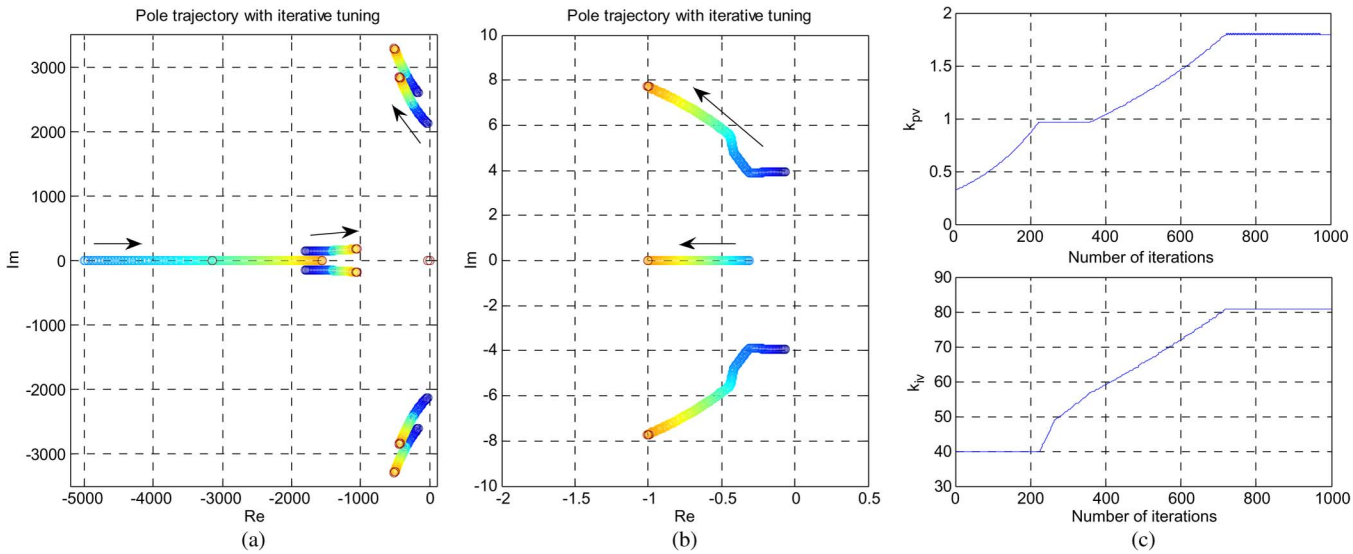

Fig. 6. Result of running the tuning algorithm for 1000 iteration cycles. (a) Pole trajectory from the optimization. (b) Zoom of the pole trajectory. (c) Resulting change of controller gains k_{pv} and k_{iv}.

TABLE II
CONTROLLER PARAMETERS WITH DIFFERENT TUNINGS

Parameter	Conventional Tuning	Proposed algorithm - 400 iterations	Proposed algorithm – 800 Iterations
Current controller gain k_{pc}	0.6366	0.6366	0.6366
Current Controller integral gain k_{ic}	20	20	20
Voltage controller gain k_{pv}	0.3183	1.033	1.795
Voltage controller integral gain k_{iv}	39.79	59.00	80.79
VSM Damping coefficient k_d	10000	6530	3110
Inertia constant T_a	2 s	2 s	2 s

acts on the integral gain while leaving unchanged the proportional gain for approximately 150 iterations before it starts increasing both parameters alternately. At this point, the damping constant of the VSM is also modified when the algorithm is attempting to simultaneously move the three slowest poles.

The tuning algorithm is, in this case, primarily acting on the voltage controller parameters and the damping constant of the VSM, whereas the current controller parameters are left unchanged. It should be noted that if the tuning algorithm is acting on the current controller parameters, care must be taken to avoid that the current controller bandwidth is not pushed too close to the switching frequency.

B. Verification by Time-Domain Simulations

The performance of the system with the controller parameters resulting from 400 and 800 iterations of the proposed algorithm has been compared by the simulation of the system with parameters resulting from the conventional tuning procedure with a equal to 4. The resulting controller parameters for the three different cases are listed in Table II.

The simulation study has been conducted with Matlab/Simulink SimPowerSystems, based on the system configuration in Fig. 1 and the control system in Fig. 2 by using

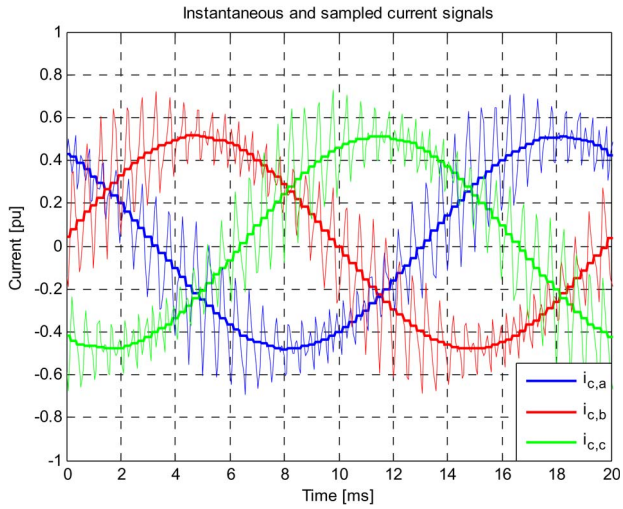

Fig. 7. Instantaneous currents in the filter inductors and the sampled values used by the control system.

the system parameters in Table I. A switching model of the converter has been used for the detailed time-domain simulation, and the sampling effects resulting from the discrete-time implementation of the control system are considered. Synchronized sampling with a double update rate has been assumed for the control system, and a switching frequency of 2 kHz therefore corresponds to a sampling frequency of 4 kHz [26]. The resulting instantaneous currents in the filter inductor L_1 during the steady-state operation and the corresponding sampled current values that are used in the control system and transformed into the VSM-oriented SRF are shown in Fig. 7.

For the simulation of the three cases with the parameters in Table II, the system has been first brought to the steady state in a condition with a grid voltage of 0.95 p.u. before it is stepped back to 1.0 p.u. In the following figures, the results from the detailed simulation model are also compared with the results from the continuous-time simulation of the linearized small-signal state-space model to verify the validity of the

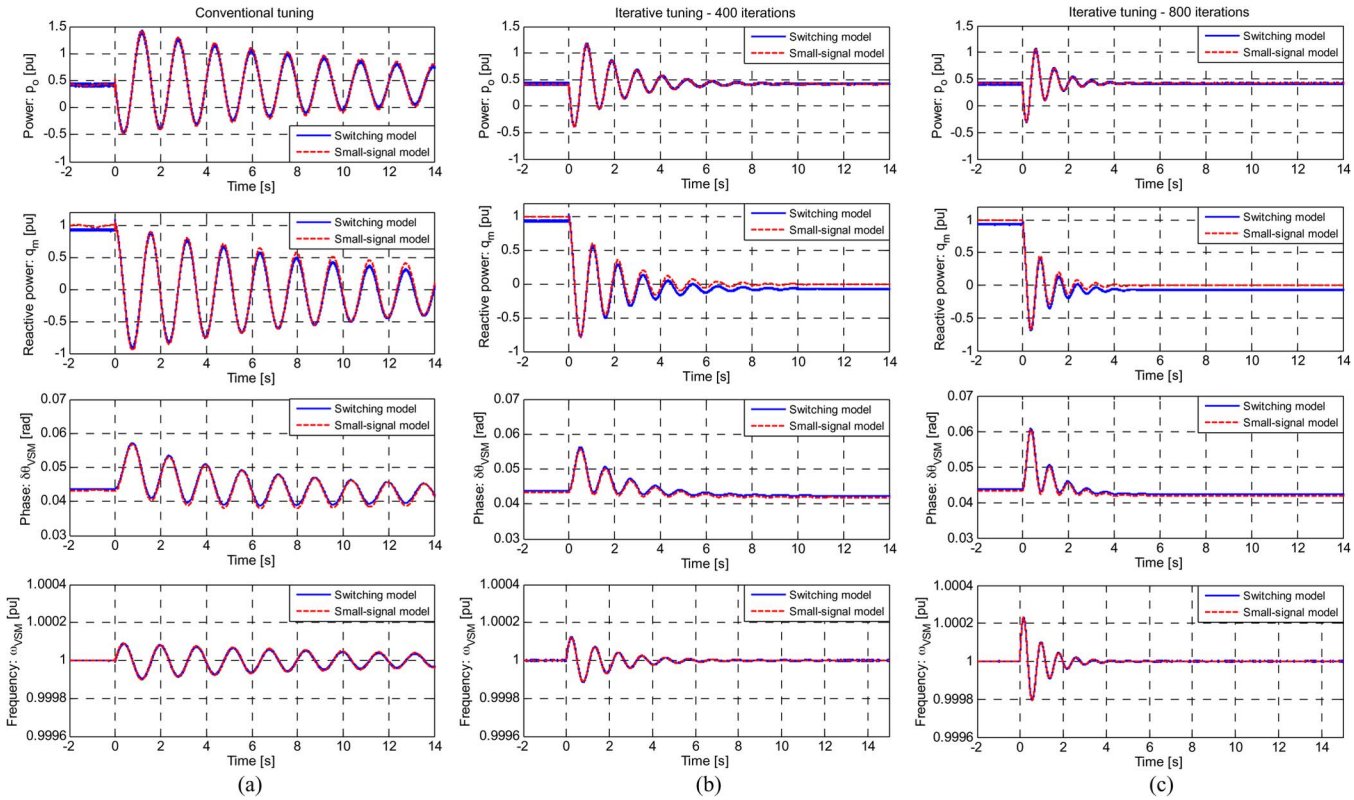

Fig. 8. Response to a step in the power reference for the investigated system with two different sets of parameters obtained with the (a) conventional tuning approach from Section III and Table I, (b) 400 iterations of the tuning algorithm, and (c) 800 iterations of the tuning algorithm.

modeling approach used for the implementation of the tuning algorithm.

The dynamic response of the system with the parameters obtained from the conventional tuning approach is shown in Fig. 8(a). In this figure, the presence of a poorly damped low-frequency oscillation can be observed in all system variables. It can be also easily verified that the observed oscillation frequency of about 0.625 Hz ($= 3.93$ rad/s) is directly corresponding to the eigenvalue of $-0.07 \pm j3.93$ analyzed in Fig. 4(b). Thus, these oscillations have a very low damping ratio of 0.018, resulting in a settling time of about 60 s. In this figure, it can be also seen that there is an excellent match between the results obtained with the detailed simulation model and the simulation of the linearized state-space model. Except for the influence of some minor noise in the signals resulting from the sampled control system, the main difference between the two models is a small deviation in the phase angle due to the delays of the sampling and the PWM output from the control system. This results in a small steady-state deviation in the reactive current and the reactive power flow, but it does not significantly influence the representation of the dynamic response and oscillation frequencies observed in the system.

From the simulations with the parameters obtained after 400 iterations of the proposed algorithm, as shown in Fig. 8(b), it is clearly demonstrated how the damping ratio of the oscillations has been significantly improved. In this case, the critical oscillatory eigenvalue resulting from the tuning algorithm has been moved to $-0.48 \pm j5.74$, resulting in an oscillation frequency of about 0.9 Hz and a damping ratio of 0.08. This theoretically corresponds to a settling time of about 8.4 s, which can be seen to match very well with the results in Fig. 8(b). Thus, the stability properties and the settling time of the system have been already significantly improved.

The results from the simulations with the parameters obtained with 800 iterations of the tuning algorithm are shown in Fig. 8(c), and it can be seen that the settling time of the system is further improved. In this case, the critical oscillatory eigenvalue is given by $-1.00 \pm j7.72$, corresponding to a damping ratio of about 0.13 and a settling time of about 4 s, which again match well with the results from the detailed simulation model.

From the presented results, it is clear that the proposed algorithm is effective in ensuring the stability and improving the dynamic performance of the system. Thus, the set of parameters obtained with the presented algorithm leads to significantly improved performance compared with what can be achieved by traditional tuning approaches when the switching frequency of the converter is relatively low. However, the traditional approach can be still useful to define the initial starting point of the proposed algorithm, whereas significant experience-based trial and error can be avoided. It can be also noted that it is difficult to move the slow real pole identified in the system beyond the location obtained after about 800 iterations. However, it could be possible to move the two complex poles further toward the left if the slowest real pole was allowed to stay in its location or possibly move slightly toward the right. This will require a more complicated algorithm that can favor the movement of eigenvalues in particular locations

when selecting the parameters to modify and is left for future investigations.

VII. Conclusion

This paper has investigated how the eigenvalue parametric sensitivities of a linearized small-signal state-space model of a power converter and its control system can be systematically utilized for the tuning of cascaded control loops. On this basis, an iterative tuning algorithm for ensuring the stability and improving the dynamic response of a power converter control system with multiple cascaded loops has been developed. This algorithm uses the eigenvalue parametric sensitivities to identify the parameters with the strongest influence on the critical eigenvalues of the system and incrementally modifies the tunable parameters in the system so that these eigenvalues are moved toward the left. The proposed algorithm has been applied to a VSM based on cascaded voltage and current controllers in the SRF. It has been shown how the proposed tuning algorithm can be used to ensure the stability of the system and significantly improve the dynamic response beyond what is achievable with a conventional rule-based approach with corresponding approximations. The obtained performance improvements have been verified by time-domain simulations, including the switching effects of the power converter and the sampling effects resulting from a discrete-time control system implementation.

References

[1] J. Rocabert, A. Luna, F. Blaabjerg, and P. Rodríguez, "Control of power converters in AC microgrids," *IEEE Trans. Power Electron.*, vol. 27, no. 11, pp. 4734–4749, Nov. 2012.

[2] T. C. Green and M. Prodanović, "Control of inverter-based micro-grids," *Elect. Power Syst. Res.*, vol. 77, no. 9, pp. 1204–1213, Jul. 2007.

[3] M. C. Chandorkar, D. M. Divan, and R. Adapa, "Control of parallel connected inverters in standalone ac supply systems," *IEEE Trans. Ind. Appl.*, vol. 29, no. 1, pp. 136–143, Jan./Feb. 1993.

[4] J. M. Guerrero, L. G. de Vicuña, J. Miret, J. Matas, and J. Cruz, "Output impedance performance for parallel operation of UPS inverters using wireless and average current-sharing controllers," in *Proc. IEEE 35th Annu. Power Electron. Spec. Conf.*, Aachen, Germany, Jun. 20–25, 2004, pp. 2482–2488.

[5] J. C. Vasquez, J. M. Guerrero, A. Luna, P. Rodríguez, and R. Teodorescu, "Adaptive droop control applied to voltage-source inverters operating in grid-connected and islanded modes," *IEEE Trans. Ind. Electron.*, vol. 56, no. 10, pp. 4088–4096, Oct. 2009.

[6] W. Leonhard, *Control of Electrical Drives*. Heidelberg, Germany: Springer-Verlag, 1985.

[7] C. Bajracharya, M. Molinas, J. A. Suul, and T. M. Undeland, "Understanding of tuning techniques of converter controllers for HVDC," in *Proc. NORPIE*, Helsinki, Finland, Jun. 9–11, 2008, pp. 1–8.

[8] J. A. Suul, M. Molinas, L. Norum, and T. Undeland, "Tuning of control loops for grid connected voltage source converters," in *Proc. 2nd IEEE Power Energy Conf.*, Johor Baharu, Malaysia, Dec. 1–3, 2008, pp. 797–802.

[9] P. Kundur, *Power System Stability and Control*. New York, NY, USA: McGraw-Hill, 1994.

[10] N. Bottrell, M. Prodanovic, and T. C. Green, "Dynamic stability of a microgrid with an active load," *IEEE Trans. Power Electron.*, vol. 28, no. 11, pp. 5107–5119, Nov. 2013.

[11] R. Majumder, "Some aspects of stability in microgrids," *IEEE Trans. Power Syst.*, vol. 28, no. 3, pp. 3243–3252, Aug. 2013.

[12] F. Katiraei, M. R. Iravani, and P. W. Lehn, "Small-signal dynamic model of a micro-grid including conventional and electronically interfaced distributed resources," *IET Gener. Transmiss. Distrib.*, vol. 1, no. 3, pp. 369–378, May 2007.

[13] Y. A.-R. I. Mohamed and E. F. El-Saadany, "Adaptive decentralized droop controller to preserve power sharing stability of paralleled inverters in distributed generation microgrids," *IEEE Trans. Power Electron.*, vol. 23, no. 6, pp. 2806–2816, Nov. 2008.

[14] N. Pogaku, M. Prodanović, and T. C. Green, "Modeling, analysis and testing of autonomous operation of an inverter-based microgrid," *IEEE Trans. Power Electron.*, vol. 22, no. 2, pp. 613–625, Mar. 2007.

[15] S. Danielsen, O. B. Fosso, and T. Toftevaag, "Use of participation factors and parameter sensitivities in the study and improvement of low-frequency stability between electric rail vehicle and power supply," in *Proc. 13th EPE*, Barcelona, Spain, Sep. 8–10, 2009, pp. 1–10.

[16] S. Danielsen, "Electric traction power system stability—Low-frequency interaction between advanced rail vehicles and a rotary frequency converter," Ph.D. thesis, Dept. Elect. Power Eng., Norwegian Univ. Sci. Technol., 2010.

[17] S. D'Arco, J. A. Suul, and O. B. Fosso, "Control system tuning and stability analysis of virtual synchronous machines," in *Proc. IEEE ECCE*, Denver, CO, USA, Sep. 15–19, 2013, pp. 2664–2671.

[18] H.-P. Beck and R. Hesse, "Virtual synchronous machine," in *Proc. 9th Int. Conf. Elect. Power Qual. Utilisation*, Barcelona, Spain, Oct. 9–11, 2007, pp. 1–6.

[19] Y. Chen, R. Hesse, D. Turschner, and H.-P. Beck, "Investigation of the virtual synchronous machine in the island mode," in *Proc. 3rd IEEE Innov. Smart Grid Technol. Eur. Conf.*, Berlin, Germany, Oct. 15–17, 2012, pp. 1–6.

[20] Y. Chen, R. Hesse, D. Turschner, and H.-P. Beck, "Dynamic properties of the virtual synchronous machine (VSIMA)," in *Proc. ICREPQ*, Las Palmas, Spain, Apr. 13–15, 2011, pp. 1–5.

[21] Q.-C. Zhong and G. Weiss, "Synchronverters: Inverters that mimic synchronous generators," *IEEE Trans. Ind. Electron.*, vol. 58, no. 4, pp. 1259–1267, Apr. 2011.

[22] S. D'Arco and J. A. Suul, "Virtual synchronous machines—Classification of implementations and analysis of equivalence to droop controllers for microgrids," in *Proc. IEEE PowerTech Grenoble*, Grenoble, France, Jun. 16–20, 2013, pp. 1–7.

[23] S. D'Arco and J. A. Suul, "Equivalence of virtual synchronous machines and frequency-droops for converter-based microgrids," *IEEE Trans. Smart Grid*, vol. 5, no. 1, pp. 394–395, Jan. 2014.

[24] V. Blasko and V. Kaura, "A new mathematical model and control of a three-phase AC–DC voltage source converter," *IEEE Trans. Power Electron.*, vol. 12, no. 1, pp. 116–123, Jan. 1997.

[25] F. Garofalo, L. Iannelli, and F. Vasca, "Participation factors and their connections to residues and relative gain array," in *Proc. 15th Triennal World Congr. Int. Fed. Automat. Control*, Barcelona, Spain, Jul. 21–26, 2002, p. 180.

[26] S. Buso and P. Mattavelli, *Digital Control in Power Electronics*. Princeton, NJ, USA: Morgan & Claypool, 2006.

Salvatore D'Arco received the M.Sc. and Ph.D. degrees in electrical engineering from the University of Naples Federico II, Naples, Italy, in 2002 and 2005, respectively.

From 2006 to 2007, he was a Postdoctoral Researcher with the University of South Carolina, Columbia, SC, USA. In 2008, he joined ASML Holding N.V., Veldhoven, The Netherlands, where he worked as a Power Electronics Designer until 2010. From 2010 to 2012, he was a Postdoctoral Researcher with the Department of Electric Power Engineering, Faculty of Information Technology, Mathematics and Electrical Engineering, Norwegian University of Science and Technology, Trondheim, Norway. In 2012, he joined SINTEF Energy Research, Trondheim, Norway, where he currently works as a Research Scientist. He is the author of over 50 scientific papers, and he is the holder of one patent. His main research activities are related to the control and analysis of power electronic conversion systems for power system applications, including the real-time simulation and rapid prototyping of converter control systems.

Jon Are Suul (M'11) received the M.Sc. and Ph.D. degrees from the Norwegian University of Science and Technology (NTNU), Trondheim, Norway, in 2006 and 2012, respectively.

From 2006 to 2007, he was with SINTEF Energy Research, Trondheim, Norway, where he was engaged in the simulation of power electronic systems until starting his Ph.D. studies. In 2008, he was a Guest Ph.D. Student for two months with the Energy Technology Research Institute, National Institute of Advanced Industrial Science and Technology, Tsukuba, Japan. In 2010, he was also a Visiting Ph.D. Student for two months with the Research Center on Renewable Electrical Energy Systems, Department of Electrical Engineering, Technical University of Catalonia, Terrassa, Spain. Since 2012, he has resumed a part-time position as a Research Scientist with SINTEF Energy Research while also working as a part-time Postdoctoral Researcher with the Department of Electric Power Engineering, Faculty of Information Technology, Mathematics and Electrical Engineering, NTNU. His research interests are mainly related to the control of power electronic converters in power systems and for renewable energy applications.

Olav Bjarte Fosso (M'90–SM'06) received the M.Sc. degree in electrical engineering and the Ph.D. degree from the Norwegian Institute of Technology, Trondheim, Norway, in 1985 and 1989, respectively.

From 1989 to 2002, he was with SINTEF Energy Research, working with the development of methods and principles for the utilization of renewable energy in electricity markets and for transmission network utilization. Since 2002, he has been a Professor with the Department of Electric Power Engineering, Faculty of Information Technology, Mathematics and Electrical Engineering, Norwegian University of Science and Technology (NTNU), Trondheim, Norway, where he served as the Head of the department from 2009 to 2013 and is currently the Director of the thematic area "Energy." His main research interests include offshore grids and the market integration of intermittent generation.

Dr. Fosso is a member of the International Council on Large Electric Systems (CIGRE) and served as the Chairman of the SC C5 on Electricity Markets and Regulation in 2008–2014. He is NTNU's Board Member for the Norwegian Research Centre for Offshore Wind Technology (NOWITECH).